2011

Luminosities of recycled radio pulsars in globular clusters

Manjari Bagchi

D. R. Lorimer

Jayanth Chennamangalam

Monthly Notices
of the
ROYAL ASTRONOMICAL SOCIETY

Mon. Not. R. Astron. Soc. **418,** 477–489 (2011) doi:10.1111/j.1365-2966.2011.19498.x

Luminosities of recycled radio pulsars in globular clusters

Manjari Bagchi,[1⋆] D. R. Lorimer[1,2] and Jayanth Chennamangalam[1]

[1]*Department of Physics, 210 Hodges Hall, West Virginia University, Morgantown, WV 26506, USA*
[2]*National Radio Astronomy Observatory, Green Bank Observatory, PO Box 2, Green Bank, WV 24944, USA*

Accepted 2011 July 21. Received 2011 June 25; in original form 2011 April 27

ABSTRACT

Using Monte Carlo simulations, we model the luminosity distribution of recycled pulsars in globular clusters as the brighter, observable part of an intrinsic distribution. We find that the observed luminosities can be reproduced using either lognormal or power-law distributions as the underlying luminosity function. For both distributions, a wide range of model parameters provide an acceptable match to the observed sample, with the lognormal function providing statistically better agreement in general than the power-law models. Moreover, the power-law models predict a parent population size that is a factor of between 2 and 10 times higher than for the lognormal models. We note that the lognormal luminosity distribution found for the normal pulsar population by Faucher-Giguère and Kaspi is consistent with the observed luminosities of globular cluster pulsars. For Terzan 5, our simulations show that the sample of detectable radio pulsars, and the diffuse radio flux measurement, can be explained using the lognormal luminosity law with a parent population of ∼150 pulsars. Measurements of diffuse gamma-ray fluxes for several clusters can be explained by both power-law and lognormal models, with the lognormal distributions again providing a better match in general. In contrast to previous studies, we do not find any strong evidence for a correlation between the number of pulsars inferred in globular clusters and globular cluster parameters, including metallicity and stellar encounter rate.

Key words: methods: numerical – methods: statistical – stars: neutron – pulsars: general – globular clusters: general – globular clusters: individual: Terzan 5.

1 INTRODUCTION

The first millisecond radio pulsar in a globular cluster (GC) was discovered by Lyne et al. (1987), shortly after earlier predictions that the putative progenitors of millisecond pulsars (MSPs) are low-mass X-ray binaries (Alpar et al. 1982), which are known to be present in GCs (Katz 1975). Inspired by this discovery, a large number of sensitive pulsar searches have been performed since then, resulting in the currently observed population of 143 radio pulsars in 27 GCs.[1] GCs have some physical properties that are different from those of the Galactic disc (e.g. an extremely high stellar density and a high abundance of metal-poor Population II stars, which indicate that they were born in the early phase of the Galaxy's formation). These facts lead naturally to the question of whether the population of radio pulsars in GCs is different to their counterparts in the Galactic disc. A number of the differences are already well known – in particular, the high abundance of MSPs, both in eccentric binary systems and as isolated objects. These phenomena can be explained as the results of two-body or three-body stellar interactions in the dense stellar environment of GCs (Romani, Kulkarni & Blandford 1987; Verbunt et al. 1987; Ivanova et al. 2008; Bagchi & Ray 2009). However, the luminosity of a pulsar is a more fundamental property because it can, in principle, be linked to the pulsar emission mechanism. It is therefore important to establish whether there is any evidence that MSPs have a different luminosity function in the disc compared to those in GCs.

There are two main ways to determine the pulsar luminosity function numerically: (i) a full dynamical approach; (ii) a snapshot approach. In the dynamical approach, a simulation is performed in which a model Galaxy of pulsars is seeded according to various prescriptions of birth locations and initial rotational parameters. Each of these synthetic pulsars is then 'evolved' both kinematically in a model for the Galactic gravitational potential and rotationally using a model for neutron star spin-down. The resulting population is then passed through the various detection criteria (see, for example, Faucher-Giguère & Kaspi 2006, hereafter FK06). The resulting set of 'detectable' pulsars is then compared to the observed sample. The snapshot approach differs from the dynamical approach in that the pulsars are seeded at their final positions in the Galaxy without assuming anything about their spin-down or kinematic evolution. Thus, they form a picture of the present-day population.

⋆E-mail: Manjari.Bagchi@mail.wvu.edu

[1] For a complete list, see Paulo C. Freire's catalogue for pulsars in globular cluster at http://www.naic.edu/∼pfreire/GCpsr.html.

The dynamical approach has been used extensively to study normal pulsars in the Galactic disc (Bhattacharya et al. 1992; Gonthier et al. 2002; FK06; Ridley & Lorimer 2010). In these studies, the luminosity of pulsars was considered to be described by power-law functions involving P and $\dot{P}$, with a substantial dispersion to account for distance uncertainties and beam geometry. One of the conclusions by FK06, also verified by Ridley & Lorimer (2010), is that the resulting parent population of luminosities appears to be well described by a lognormal function. As discussed further in Section 3.1, the lognormal parameters favoured by FK06 (for the base-10 logarithm of the 1400-MHz luminosities) are a mean of -1.1 and a standard deviation of 0.9. One of the goals of the current study is to examine whether these lognormal parameters are consistent with the observed populations of GC pulsars.

For pulsars in GCs, where it is difficult to model the effects of stellar encounters and the cluster potential, the dynamical approach has so far not been used for radio pulsar population syntheses. Although it might be possible to use such an approach in the future, in this work we adopt a version of the snapshot approach. We carry out Monte Carlo simulations, which assume that all GCs have the same intrinsic pulsar luminosity function, but a different population size. We use this approach to model the observed sample of pulsars, given the various ranges of luminosities. As can be seen, this approach provides a remarkably good agreement between the model and observed luminosity distributions.

Within the snapshot framework, the complementary cumulative distribution function (CCDF) of pulsar luminosity is usually fit as a power law as $N(>L_{1400}) = N_0 L_{1400}^{\mathrm{q}}$, where L_{1400} is the luminosity of the pulsar at 1400 MHz, N is the number of pulsars having a luminosity value greater than L_{1400} and N_0 and q are constants. We note here that sometimes in the literature (Hessels et al. 2007; Hui, Cheng & Taam 2010, hereafter HCT10), the CCDF has been mentioned as the cumulative distribution function (CDF). However, the CDF $[N(\leqslant L_{1400})]$ is actually related to the CCDF as CDF $=$ $1 -$ CCDF. Using this snapshot technique, HCT10 concluded that the luminosities of MSPs in GCs are different from those in the Galactic disc because the CCDF for GC MSPs is much steeper than that of disc pulsars. This is a very important conclusion. If correct, it would imply that the radio luminosity is related to differences in formation processes between the disc and GC pulsars. The same analysis was also performed with more recent distance estimates of GCs, and the resultant CCDF was even steeper (Bagchi & Lorimer 2010).

Because GCs are generally at large distances, the luminosity function of observed pulsars is not as well sampled as in the Galactic disc. In the present work, we try to account for this incompleteness by considering GC MSPs as the brighter tail of some intrinsic parent population. The goal of the current work is to explore the range of possible distributions that are consistent with the current sample of GC pulsars. The plan for the rest of this paper is as follows. In Section 2, we describe the pulsar sample we use. In Section 3, we present our analysis procedure and its main results. In Section 4, we investigate additional constraints on allowed model parameters from observations of diffuse radio and gamma-ray flux. In Section 5, we compare our results with earlier work. We draw our main conclusions in Section 6.

2 OBSERVATIONAL SAMPLE

The luminosity of a pulsar, L, can be computed (see, for example, Lorimer & Kramer 2005) from its distance and the mean flux density S_ν (defined at some observing frequency ν) using the following geometrical relationship:

$$L = \frac{4\pi d^2}{\delta} \sin^2\left(\frac{\rho}{2}\right) \int_{\nu_{\mathrm{low}}}^{\nu_{\mathrm{up}}} S_\nu \, \mathrm{d}\nu. \quad (1)$$

Here, ρ is the radius of the (assumed circular) emission cone, δ is the pulse duty cycle ($=W_{\mathrm{eq}}/P$, where P is the spin period of the pulsar and W_{eq} is the equivalent width of the pulse, i.e. the width of a top-hat-shaped pulse having the same area and peak flux density as the true profile), ν_{low} and ν_{up} define the range of radio frequencies over which the pulsar has been observed and d is the distance of the pulsar. As it is usually difficult to determine the values of ρ and δ reliably, we define the 'pseudo-luminosity' as follows:

$$L_\nu = S_\nu \, d^2. \quad (2)$$

Henceforth, we use the term luminosity to mean pseudo-luminosity.

Among the current sample of 143 GC pulsars, flux density values have been reported for 107 pulsars. Among these, three are clearly young isolated objects, which more closely resemble the normal population of pulsars in the Galaxy (for a further discussion of this population, see Boyles et al. 2011). We consider here the sample of 83 pulsars in 10 GCs with spin periods $P \leqslant 100$ ms with each of these GCs hosting at least four such pulsars. For all these objects, the spin and binary properties suggest that the neutron star has undergone a phase of recycling in the past.

Among these, for 45 pulsars (14 in 47 Tuc, four in M3, five in M5, five in M13, five in NGC 6752, three in NGC 6517 and nine in M28) the flux density values have been measured at 1400 MHz, for 31 pulsars (25 in Terzan 5, five in NGC 6440 and one in NGC 6517) the flux density values have been measured at 1950 MHz and for seven pulsars (in M5) the flux density values have been measured at 400 MHz. To pursue our study of pulsar luminosities at 1400 MHz, we scale the flux densities measured at other frequencies using the power law $S_\nu \propto \nu^\alpha$, where α is the spectral index. We then use the model prediction for S_{1400} as the best estimate of the pulsar's flux density at this frequency. In these calculations, we use the values of α estimated from the observed values of fluxes at different frequencies whenever available; otherwise, we adopt the mean α of GC MSPs (for which flux values have been reported at multiple frequencies) of -1.9. Toscano et al. (1998) also obtained a mean α of 19 millisecond pulsars to be -1.9 ± 0.1, but their sample contains only two GC pulsars. Once we obtain S_{1400}, we can calculate L_{1400} if d is known. For GC pulsars, the distances are taken to be those of their host clusters. We use the most recent distance estimates from the literature.

Table 1 gives our complete list of GC pulsar flux and spectral parameters used in this section and in the remainder of the paper. While compiling this list, we confirmed the earlier conclusions by Hessels et al. (2007) that the choice of α in a realistic range does not affect the complementary cumulative distribution (CCD) of luminosities significantly. Using 37 isolated GC pulsars, Hessels et al. (2007) found that an arbitrary choice of α in the range of -1.6 to -2.0 does not affect the shape of the CCD. We arrive at the same conclusion with our sample, using the following different values of α: -1.6, -1.9 and -2.2. We perform Kolmogorov–Smirnov (KS) tests between the luminosity distributions obtained with different choices of α. The KS test returns a statistic P_{KS}, which gives the probability that the two samples are drawn from the same distribution (for details, see Press et al. 2007). In this case, P_{KS} is always greater than 0.997 when we compare any two luminosity distributions from the three obtained with $\alpha = -1.6$, -1.9 and -2.0; as an example, the distribution obtained with $\alpha = -1.9$ is shown in Fig. 1.

Table 1. Fluxes and spectral indices of 107 pulsars in GCs. α can be calculated for 20 pulsars using the central frequency of observations (whenever reported). Mean α of pulsars having $P_s \leqslant 100$ ms is -1.865 (excluding the positive α of PSR J1836−2354A). We set $\alpha = -1.9$ in the present work. From the sample of 107 pulsars, we exclude pulsars with spin period > 100 ms. Then, we exclude pulsars for which the host GC contains less than four pulsars with $P_s \leqslant 100$ ms and known flux values. Pulsars that are not used in the present study have been written in italic font. The references used in the table are listed in the notes at the end of the table.

GC	PSR	P_s (ms)	S_{400} (mJy)	S_{600} (mJy)	S_{1170} (mJy)	S_{1400} (mJy)	S_{1600} (mJy)	S_{1950} (mJy)	α
47 Tuc	J0023−7204C	5.757	1.53(r1)	1.54(r1)	–	*0.36*(r2)	–	–	−1.352
47 Tuc	J0024−7204D	5.358	0.95(r1)	0.55(r1)	–	*0.22*(r2)	–	–	−1.264
47 Tuc	J0024−7205E	3.536	–	–	–	0.21(r2)	–	–	–
47 Tuc	J0024−7204F	2.624	–	–	–	0.15(r2)	–	–	–
47 Tuc	J0024−7204G	4.040	–	–	–	0.05(r2)	–	–	–
47 Tuc	J0024−7204H	3.210	–	–	–	0.09(r2)	–	–	–
47 Tuc	J0024−7204I	3.485	–	–	–	0.09(r2)	–	–	–
47 Tuc	J0023−7203J	2.101	–	–	–	0.54(r2)	–	–	–
47 Tuc	J0024−7204L	4.346	–	–	–	0.04(r2)	–	–	–
47 Tuc	J0023−7205M	3.677	–	–	–	0.07(r2)	–	–	–
47 Tuc	J0024−7204N	3.054	–	–	–	0.03(r2)	–	–	–
47 Tuc	J0024−7204O	2.643	–	–	–	0.10(r2)	–	–	–
47 Tuc	J0024−7204Q	4.033	–	–	–	0.05(r2)	–	–	–
47 Tuc	J0024−7203U	4.343	–	–	–	0.06(r2)	–	–	–
NGC 1851	*J0514−4002*	4.990	0.28(r3)	–	–	–	–	0.0056(r3)	−2.568
M53	*B1310+18*	33.163	1.0(r4)	–	–	–	–	–	–
M3	J1342+2822A	2.545	–	–	–	0.007(r5)	–	–	–
M3	J1342+2822B	2.389	–	–	–	0.014(r5)	–	–	–
M3	J1342+2822C	2.166	–	–	–	0.006(r5)	–	–	–
M3	J1342+2822D	5.443	–	–	–	0.010(r5)	–	–	–
M5	B1516+02A	5.554	0.5(r6)	–	0.155(r7)	0.120(r5)	–	–	−1.161
M5	B1516+02B	7.947	0.3(r6)	–	0.027(r7)	0.025(r5)	–	–	−2.132
M5	J1518+0204C	2.484	–	–	–	0.039(r5)	–	–	–
M5	J1518+0204D	2.988	–	–	–	0.008(r5)	–	–	–
M5	J1518+0204E	3.182	–	–	–	0.010(r5)	–	–	–
M4	*B1620−26*	11.076	15(r8)	7.2(r9)	–	1.6(r10)	–	–	−1.744
M13	B1639+36A	10.378	3.0(r4)	–	–	0.140(r5)	–	–	−2.486
M13	B1639+36B	3.528	–	–	–	0.022(r5)	–	–	–
M13	J1641+3627C	3.722	–	–	–	0.030(r5)	–	–	–
M13	J1641+3627D	3.118	–	–	–	0.024(r5)	–	–	–
M13	J1641+3627E	2.487	–	–	–	0.010(r5)	–	–	–
M62	*J1701−3006A*	5.242	–	–	–	0.4(r11)	–	–	–
M62	*J1701−3006B*	3.594	–	–	–	0.3(r11)	–	–	–
M62	*J1701−3006C*	7.613	–	–	–	0.3(r11)	–	–	–
NGC 6342	*B1718−19*	1004.04	0.253(r12)	0.550(r12)	–	0.278(r12)	0.18(r12)	–	−0.338
NGC 6397	*J1740−5340*	3.650	–	–	–	1.0(r13)	–	–	–
Ter 5	J1748−2446A	11.563	–	5(r14)	–	0.61(r15)	–	1.020(r16)	−1.572
Ter 5	J1748−2446C	8.436	–	–	–	–	–	0.360(r16)	–
Ter 5	J1748−2446D	4.714	–	–	–	–	–	0.041 (r16)	–
Ter 5	J1748−2446E	2.198	–	–	–	–	–	0.048(r16)	–
Ter 5	J1748−2446F	5.540	–	–	–	–	–	0.035(r16)	–
Ter 5	J1748−2446G	21.672	–	–	–	–	–	0.015(r16)	–
Ter 5	J1748−2446H	4.926	–	–	–	–	–	0.015(r16)	–
Ter 5	J1748−2446I	9.570	–	–	–	–	–	0.029(r16)	–
Ter 5	J1748−2446J	80.338	–	–	–	–	–	0.019(r16)	–
Ter 5	J1748−2446K	2.970	–	–	–	–	–	0.040(r16)	–
Ter 5	J1748−2446L	2.245	–	–	–	–	–	0.041(r16)	–
Ter 5	J1748−2446M	3.570	–	–	–	–	–	0.033(r16)	–
Ter 5	J1748−2446N	8.667	–	–	–	–	–	0.055(r16)	–
Ter 5	J1748−2446O	1.677	–	–	–	–	–	0.120(r16)	–

Table 1 *–Continued*

GC	PSR	P_s (ms)	S_{400} (mJy)	S_{600} (mJy)	S_{1170} (mJy)	S_{1400} (mJy)	S_{1600} (mJy)	S_{1950} (mJy)	α
Ter 5	J1748−2446P	1.729	–	–	–	–	–	0.077(r16)	–
Ter 5	J1748−2446Q	2.812	–	–	–	–	–	0.027(r16)	–
Ter 5	J1748−2446R	5.028	–	–	–	–	–	0.012(r16)	–
Ter 5	J1748−2446S	6.117	–	–	–	–	–	0.018(r16)	–
Ter 5	J1748−2446T	7.085	–	–	–	–	–	0.020(r16)	–
Ter 5	J1748−2446U	3.289	–	–	–	–	–	0.016(r16)	–
Ter 5	J1748−2446V	2.072	–	–	–	–	–	0.071(r16)	–
Ter 5	J1748−2446W	4.205	–	–	–	–	–	0.022(r16)	–
Ter 5	J1748−2446X	2.999	–	–	–	–	–	0.018(r16)	–
Ter 5	J1748−2446Y	2.048	–	–	–	–	–	0.016(r16)	–
Ter 5	J1748−2446ad	1.396	–	–	–	–	–	0.08(r17)	–
NGC 6440	*B1745−20*	288.603	10(r18)	–	–	0.37(r15)	1.5(r18)	0.37(r19)	−1.920
NGC 6440	J1748−2021B	16.760	–	–	–	–	–	0.047(r19)	–
NGC 6440	J1748−2021C	6.227	–	–	–	–	–	0.044(r19)	–
NGC 6440	J1748−2021D	13.496	–	–	–	–	–	0.075(r19)	–
NGC 6440	J1748−2021E	16.264	–	–	–	–	–	0.023(r19)	–
NGC 6440	J1748−2021F	3.794	–	–	–	–	–	0.017(r19)	–
NGC 6441	*J1750−37A*	111.608	–	–	–	–	–	0.059(r19)	–
NGC 6441	*J1750−3703B*	6.074	–	–	–	–	–	0.037(r19)	–
NGC 6441	*J1750−3703C*	26.569	–	–	–	–	–	0.015(r19)	–
NGC 6441	*J1750−3703D*	5.140	–	–	–	–	–	0.010(r19)	–
NGC 6517	J1801−0857A	7.176	–	–	–	0.036(r20)	–	0.020(r20)	−1.648
NGC 6517	J1801−0857B	28.961	–	–	–	0.012(r20)	–	0.009(r20)	−0.806
NGC 6517	J1801−0857C	3.739	–	–	–	0.012(r20)	–	0.007(r20)	−1.511
NGC 6517	J1801−0857D	4.226	–	–	–	–	–	0.011(r20)	–
NGC 6539	*B1802−07*	23.101	3.1(r21)	1.0(r21)	–	0.6 (r21)	–	–	−1.213
NGC 6544	*J1807−2459A*	3.059	–	–	–	1.3(r22)	–	–	–
NGC 6624	*B1820−30A*	5.440	16(r9)	6.8(r9)	–	0.72(r9)	0.31(r23)	–	−2.922
NGC 6624	*B1820−30B*	378.596	2.2(r21)	1.0(r21)	–	0.07(r23)	0.07(r23)	–	−2.654
M28	B1821−24A	3.054	30(r24)	–	–	0.94(r25)	–	–	−2.764
M28	J1824−2452B	6.547	–	–	–	0.07(r25)	–	–	–
M28	J1824−2452C	4.159	–	–	–	0.17(r25)	–	–	–
M28	J1824−2452D	79.832	–	–	–	0.05(r25)	–	–	–
M28	J1824−2452E	5.420	–	–	–	0.06(r25)	–	–	–
M28	J1824−2452F	2.451	–	–	–	0.08(r25)	–	–	–
M28	J1824−2452G	5.909	–	–	–	0.05(r25)	–	–	–
M28	J1824−2452H	4.629	–	–	–	0.06(r25)	–	–	–
M28	J1824−2452J	4.039	–	–	–	0.07(r25)	–	–	–
M22	*J1836−2354A*	3.354	–	–	–	0.040(r20)	–	0.043(r20)	0.203
M22	*J1836−2354B*	3.232	–	–	–	0.200(r20)	–	0.073(r20)	−2.826
NGC 6749	J1905+0154A	3.193	–	–	–	0.023(r5)	–	–	–
NGC 6749	J1905+0154B	4.968	–	–	–	0.006(r5)	–	–	–
NGC 6752	J1911−5958A	3.266	–	–	–	0.21(r26)	–	–	–
NGC 6752	J1910−5959B	8.358	–	–	–	0.05(r26)	–	–	–
NGC 6752	J1911−6000C	5.277	–	–	–	0.24(r26)	–	–	–
NGC 6752	J1910−5959D	9.035	–	–	–	0.05(r26)	–	–	–
NGC 6752	J1910−5959E	4.572	–	–	–	0.07(r26)	–	–	–
M71	*J1953+1846A*	4.888	–	–	–	0.059(r5)	–	–	–
M15	*B2127+11A*	110.665	1.7(r27)	–	–	0.2(r28)	–	–	−1.797
M15	B2127+11B	56.133	1.0(r27)	–	–	–	–	–	–
M15	B2127+11C	30.529	0.64(r27)	–	–	–	–	–	–
M15	B2127+11D	4.803	0.34(r27)	–	–	–	–	–	–
M15	B2127+11E	4.651	0.24(r27)	–	–	–	–	–	–

Table 1. *–Continued*

GC	PSR	P_s (ms)	S_{400} (mJy)	S_{600} (mJy)	S_{1170} (mJy)	S_{1400} (mJy)	S_{1600} (mJy)	S_{1950} (mJy)	α
M15	B2127+11F	4.027	0.14(r27)	–	–	–	–	–	–
M15	B2127+11G	37.660	0.13(r27)	–	–	–	–	–	–
M15	B2127+11H	6.743	0.16(r27)	–	–	–	–	–	–
M30	*J2140−2310A*	11.019	–	–	–	0.08(r29)	–	–	–

References: r1, Robinson et al. (1995); r2, Camilo, Lorimer & Freire (2000); r3, Freire, Ransom & Gupta (2007); r4, Kulkarni et al. (1991); r5, Hessels et al. (2007); r6, Anderson et al. (1997); r7, Freire et al. (2008a); r8, unpublished (http://www.atnf.csiro.au/research/pulsar/psrcat/expert.html); r9, Toscano et al. (1998); r10, Kramer et al. (1998); r11, Possenti et al. (2003); r12, averaged over variations with the orbital phase (Lyne et al. 1993); r13, D'Amico et al. (2001); r14, Lyne et al. (1990); r15, Hobbs, Faulkner & Stairs (2004); r16, Ransom et al. (2005); r17, Hessels et al. (2006); r18, Lyne, Manchester & D'Amico (1996); r19, Freire et al. (2008b); r20, Lynch et al. (2011); r21, Lorimer et al. (1995); r22, Ransom et al. (2001); r23, Biggs et al. (1994); r24, Foster, Fairhead & Backer (1991); r25, Bégin (2006); r26, Corongiu et al. (2006); r27, Anderson (1993); r28, Wolszczan et al. (1989); r29, Ransom et al. (2004).

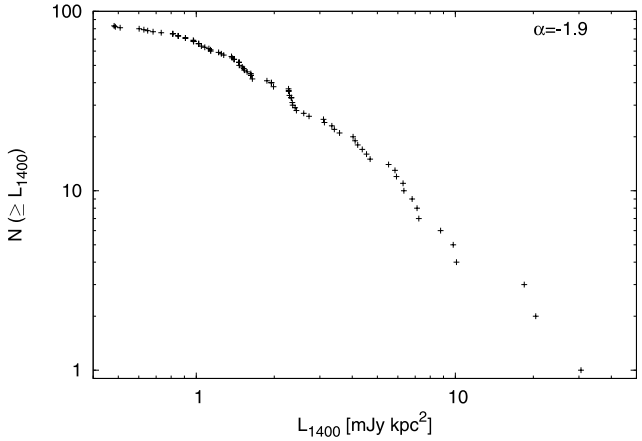

Figure 1. CCD of 1400-MHz luminosities for the sample of GC pulsars. Flux density values measured at other frequencies have been converted to S_{1400} using $S_\nu \propto \nu^\alpha$ for $\alpha = -1.9$. We have checked that a change in the value of $\alpha \sim \pm 0.3$ does not make any visible change to the shape of the plot.

The absence of any significant difference in the luminosity distribution for a realistic range of α also supports our choice of $\alpha = -1.9$ for this work, which is not too different from the choice ($\alpha = -1.8$) favoured in other studies (Maron et al. 2000; HCT10). As we are studying luminosities only at 1400 MHz, hereafter we denote L_{1400} simply by L.

Note also that, throughout this paper, we are concerned with the possible forms of the luminosity distribution of cluster pulsars. Correlations between luminosity and other pulsar parameters are not discussed in any detail here. The reason for this is that, as for the pulsar population in the Galaxy, correlations in the observed pulsar samples are not apparent because of the presence of distance errors and beaming uncertainties (see Lorimer et al. 1993, for a discussion). We did not find any correlation between the luminosity and spin period of the 83 recycled pulsars used in the present work. As mentioned earlier, $\dot{P}$ measurements for GC pulsars are affected by the cluster potential. Thus, they cannot easily be used to study the intrinsic properties of the pulsars. For the remainder of this paper, we proceed with the underlying assumption that there exists a single luminosity function for all GC pulsars, and we attempt to explain the observed luminosities in this way. As we demonstrate, the data are remarkably consistent with this simple idea. However, the wide ranges of possible model parameters that are consistent with the data do not rule out the idea that the parent luminosity function might vary from cluster to cluster.

3 ANALYSIS

With the data described in the previous section, we aim to find luminosity distribution functions whose brighter tail can be considered as the observed luminosity distribution of GC pulsars, assuming that the parent luminosity distribution is the same for all GCs. To do so, for each GC, we first generate a synthetic sample of $N_{\mathrm{trial},i}$ pulsar luminosities from a chosen distribution function until we obtain $C \times N_{\mathrm{obs},i}$ pulsars having simulated luminosities greater than the observed minimum luminosity for that GC. This multiplication by the constant C (100–1000) is done to minimize statistical variations. In this notation, i is the GC index and $N_{\mathrm{obs},i}$ is the observed number of pulsars in the GC that we consider.

$$L_{\mathrm{sim,tot}} = \frac{1}{C} \sum_{j=1}^{N_{\mathrm{trial},i}} L_{\mathrm{sim},j} \tag{3}$$

is the total luminosity and

$$S_{\mathrm{sim,tot}} = \frac{1}{C} \sum_{j=1}^{N_{\mathrm{trial},i}} S_{\mathrm{sim},j} \tag{4}$$

is the total flux in the ith GC. Here, $L_{\mathrm{sim},j}$ and $S_{\mathrm{sim},j}$ are the simulated luminosities and corresponding fluxes. After we perform the simulation for all 10 GCs, we compare the simulated luminosities with the observed luminosities of 83 pulsars by performing KS and χ^2 tests. As mentioned earlier, the KS test can be used to test the hypothesis that two distributions differ. A low value of KS probability P_{KS} suggests a mismatch. The χ^2 statistic uses binned data and compares the values of the two distributions at each bin. Here, a low value of χ^2 implies a good agreement. We divide the luminosity range 0.1–1000 mJy kpc^2 into 36 logarithmically equispaced bins. $N_{\mathrm{trial},i}/C$ is the predicted number of total pulsars in that GC, which we call $N_{\mathrm{rad},i}$.

A key assumption in our present analysis is that each GC has been searched down to the level of the faintest observable pulsar in that particular cluster. This assumption provides a good approximation to the actual survey sensitivity in each cluster, and was made primarily because of the lack of currently published detail of several of the GC surveys so far. The assumption greatly simplifies our modelling procedure, as it means that we do not have to consider

variations in sensitivity because of other factors (e.g. scintillation, eclipsing binary systems, etc.). This simple approach is appropriate for the purposes of the current work where we are simply trying to assess the range of luminosity functions compatible with the data. A more rigorous study, which takes account of the survey thresholds in detail, might well be able to narrow the range of possible model parameters found here. It should certainly be carried out when more details of the surveys are published, but it is beyond the scope of the current work.

3.1 Lognormal luminosity function

We begin by testing a lognormal luminosity function, where the probability density function (PDF) is

$$f_{\rm lognormal}(L) = \frac{\log_{10} e}{L}\frac{1}{\sqrt{2\pi\sigma^2}}\exp\left[\frac{-(\log_{10} L-\mu)^2}{2\sigma^2}\right]. \quad (5)$$

Here, as usual, μ is the mean of the distribution and σ is the standard deviation. For this choice of distribution, we find that $C = 100$ is sufficient to minimize statistical fluctuations. The variations of $P_{\rm KS}$ and χ^2 with μ and σ are shown in Fig. 2. It is clear that there is a wide range of values of μ and σ for which the simulated luminosity distributions agree well with the observed sample. For the two statistical tests, good agreement is given when $P_{\rm KS}$ has high values and when χ^2 is small. As expected, the region of the μ–σ parameter space encompassed by $P_{\rm KS} > 0.05$ is essentially the same as the contours encompassing the 95 per cent probability values around the χ^2 minimum.

For this distribution, and for the purposes of later discussion, we define three models based on particular parameter choices. Model

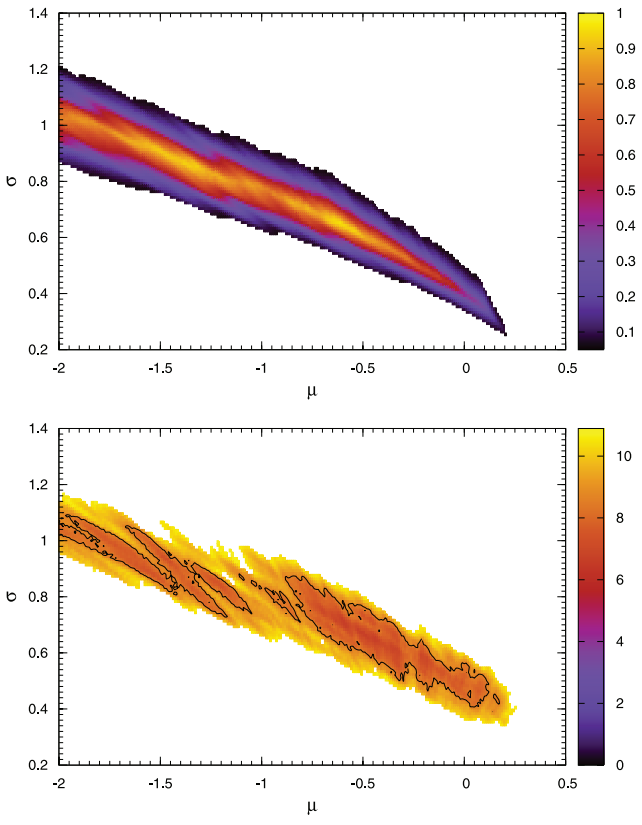

Figure 2. Top: variation of $P_{\rm KS}$ (for $P_{\rm KS} \geqslant 0.05$) with μ and σ. Bottom: variation of χ^2 (within 2σ about the minimum value of χ^2) with μ and σ, the parameters of the lognormal distribution. A 1σ contour is also shown.

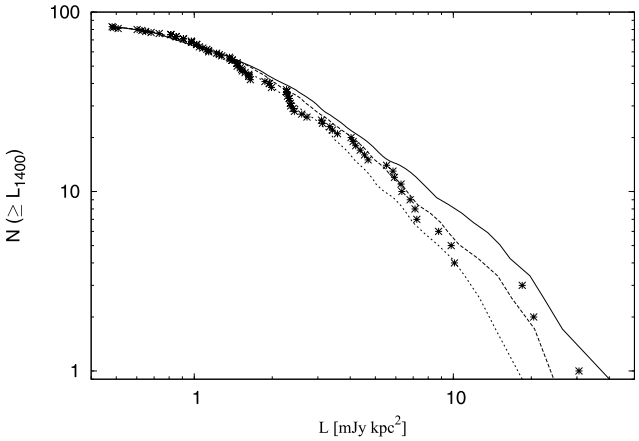

Figure 3. Observed luminosity distribution with simulated luminosity distributions generated with a lognormal distribution function for three different sets of μ and σ. These are defined as model 1 (upper curve), model 2 (lower curve) and model 3 (middle curve); see text for details. The $*$ symbols represent the observed distribution.

1 uses the parameters found by FK06 ($\mu = -1.1$ and $\sigma = 0.9$) from which we find $P_{\rm KS} = 0.15$ and $\chi^2 = 9.4$. Model 2, for which $\mu = -0.61$ and $\sigma = 0.65$, returns the maximum value of $P_{\rm KS} = 0.98$ with $\chi^2 = 7.9$. Model 3, for which $\mu = -0.52$ and $\sigma = 0.62$, returns a minimum value of $\chi^2 = 6.3$ and has $P_{\rm KS} = 0.37$.

In Fig. 3 we compare these three models with the observed data. As expected, all models match well. While model 3 provides the closest match by eye, the statistical results mentioned above do not rule out either model 1 or model 2. The FK06 luminosity model parameters (model 1) are therefore consistent with the observed CCD.

3.2 Power-law luminosity function

As mentioned earlier, power-law luminosity functions have been used by a number of authors. It is therefore of great interest to see how the power law compares to lognormal for the GC pulsars. The PDF of the power-law distribution is

$$f_{\rm power\text{-}law}(L) = \frac{\beta L_{\rm min}^{\beta}}{L^{\beta+1}}, \quad (6)$$

where $L_{\rm min}$ is the minimum value of L and β is the power-law index. This abrupt cut-off, required to avoid divergence when integrating this function over all L, is somewhat unphysical, but nevertheless can be used to parametrize the luminosities in an independent way to the lognormal. We perform simulations over a range of $L_{\rm min}$ (0.003–0.48 mJy kpc^2), as 0.48 mJy kpc^2 is the observed minimum luminosity among GC pulsars in our sample, and the lower value of $L_{\rm min}$ is chosen somewhat arbitrarily. For this model, we found that $C = 1000$ is required to minimize statistical fluctuations. Unlike the lognormal model, we found that the power-law distribution occasionally produced pulsars with large luminosities $L >> 100$ mJy kpc^2, which biased some of our preliminary simulation runs. To avoid this difficulty, we imposed a maximum luminosity of 50 mJy kpc^2. No GC pulsar is currently known with $L > 20$ mJy kpc^2, and our results are insensitive to the exact choice of the maximum luminosity cut-off over the range 20–500 mJy kpc^2.

The nominal best parameter values give $P_{\rm KS} = 0.81$ ($\chi^2 = 8.7$) for $\beta = 0.92$ and $L_{\rm min} = 0.017$ mJy kpc^2 (model 4) and minimum $\chi^2 = 8.0$ ($P_{\rm KS} = 0.56$) for $\beta = 1.01$ and $L_{\rm min} = 0.022$ mJy kpc^2 (model 5). Our values of β (which give good fits) are not too different

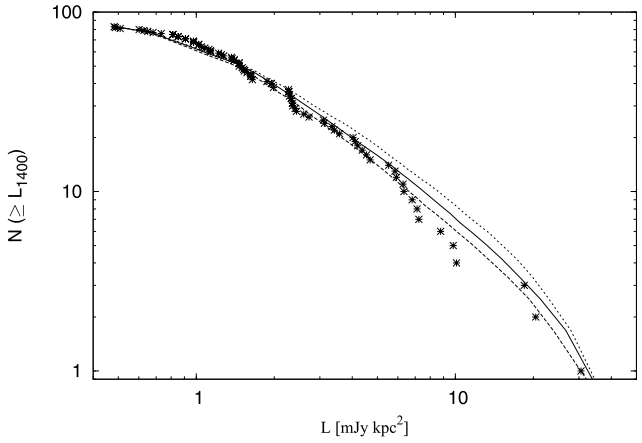

Figure 4. Observed luminosity distribution with simulated luminosity distributions generated with a power-law distribution function for three different set of $L_{\rm min}$ and β. These are defined as model 4 (middle curve), model 5 (lower curve) and model 6 (upper curve); see text for details. The $*$ symbols represent the observed distribution. The mismatch between the simulated and observed CCDs appears only when the number of pulsars are $\lesssim$10.

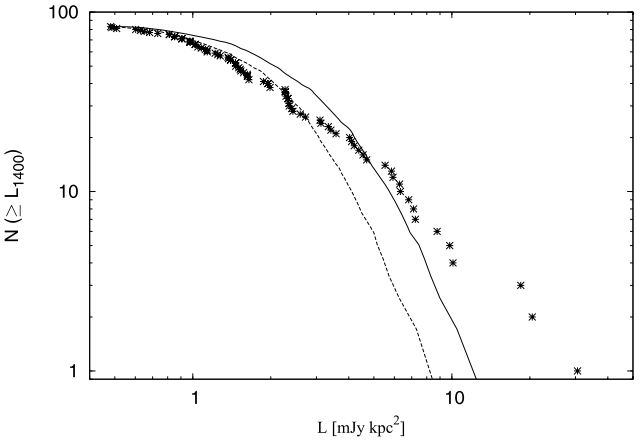

Figure 5. Observed luminosity distribution with simulated luminosity distributions generated with an exponential distribution function with $\lambda = 0.676$ mJy^{-1} kpc^{-2} (lower curve) and $\lambda = 0.439$ mJy^{-1} kpc^{-2} (upper curve). The $*$ symbols represent the observed distribution.

from the conventional values $\beta + 1 = 2$. For example, the best-fitting value of the analysis of Fruchter & Goss (2000) for Terzan 5 pulsars is $\beta + 1 = 1.85$. We have seen that for $\beta \sim 1$, the fit does not depend greatly on $L_{\rm min}$, which again agrees with the results of Fruchter & Goss (2000). As an additional point of reference, we also consider the nominal power-law parameters discussed by Fruchter & Goss (2000) (i.e. $\beta = 0.85$ and $L_{\rm min} = 0.03$ mJy kpc^2) which we refer to as model 6. For this pairing, $P_{\rm KS} = 0.43$ and $\chi^2 = 9.0$. We need to remember here that Fruchter & Goss (2000) did not put any constraint on the maximum value of the luminosity. In Fig. 4 we compare the observed CCD with simulated CCDs for models 4–6. Statistically, the agreement between simulated and observed distributions is almost as good as that for lognormal distributions.

3.3 Exponential distribution

The above models characterize the luminosity function in terms of two parameters. For completeness, we also consider a simple one-parameter model, the exponential distribution with PDF

$$f_{\rm exponential}(L_{1400}) = \lambda {\rm e}^{-\lambda L}. \quad (7)$$

Here, $1/\lambda$ is the mean of the distribution, and we find that $C = 100$ is enough to remove statistical fluctuations. For this model, the maximum value of $P_{\rm KS} = 0.17$ is obtained for $\lambda = 0.676$ mJy^{-1} kpc^{-2} with the corresponding $\chi^2 = 13.7$. The minimum value of $\chi^2 = 11.94$ is found for $\lambda = 0.439$ mJy^{-1} kpc^{-2} with $P_{\rm KS} = 0.00028$. In Fig. 5 we compare the observed CCD with the simulated CCDs for these two values of λ. It is clear that the simulated distribution never matches the observed distribution very well. Therefore, we do not consider the exponential distribution further in this work and we focus the remainder of the discussion on the lognormal and power-law distributions.

4 MODEL PREDICTIONS AND CONSTRAINTS

In Section 3, we have found that there is a large family of possible luminosity parameters that are consistent with the observed distribution of GC pulsar luminosities. These ranges translate to a variety of different predictions for the population sizes in each GC. This can be seen from a comparison of the predicted parameters for each GC using the lognormal parameter choices (models 1, 2 and 3) in Table 2 and the power-law parameter combinations (models 4, 5 and 6) in Table 3. In this section, we try to place further constraints on these parameters by examining the predictions for the diffuse radio and gamma-ray fluxes separately.

4.1 Diffuse radio emission

A potentially very useful additional constraint comes from observations of the diffuse radio emission in GCs. Assuming that the only contribution to this flux is from the pulsars, then such measurements constrain the integrated luminosity function in a given cluster. Our Monte Carlo models make specific predictions for these observations (see equation 4). For Terzan 5, the total radio flux $S_{\rm obs,tot} = 5.2$ mJy kpc^2 (the sum of diffuse flux and the fluxes of point sources) is found by Fruchter & Goss (2000). Fruchter & Goss (2000) also observed some other clusters, among which NGC 6440 belongs to our list (Table 4). However, as they mentioned that their observation in this cluster is consistent with the position of a single pulsar PSR B1745−20, we cannot use this datum for our study. For 47 Tuc, McConnell et al (2004) found[2] that $S_{\rm obs,tot} = 2.0 \pm 0.3$ mJy kpc^2.

Assuming that both the diffuse flux measurements for Terzan 5 and 47 Tuc are dominated by their respective pulsar populations, we can compare them with the predictions from our simulations. An inspection of Tables 2 and 3 shows that the observed diffuse flux for 47 Tuc is successfully reproduced by all of the models, within nominal uncertainties. For Terzan 5, the power-law models provide a better match to the diffuse flux overall, while the lognormal models predict a slightly smaller flux, which lies 2–5σ below the nominal value found by Fruchter & Goss (2000).

In Fig. 6, we fix μ to the nominal value from model 1 (i.e. as found by FK06 for normal pulsars, -1.1) and we vary σ. For this case, we see that there are only two possible ranges of σ that are compatible with the diffuse flux measurement of Terzan 5: $\sigma \sim 0.5$ or $\sigma \sim 0.9$ (see the upper panel of Fig. 6). The 'solution' with

[2] This sum is essentially equivalent to the individual fluxes of the 14 pulsars in this cluster with measured fluxes so far (see Table 1). The remaining nine currently known pulsars must therefore contribute much less than a mJy of diffuse flux. For example, a typical flux of 30 μJy per pulsar would bring the diffuse flux to ∼2.3 mJy.

Table 2. Population estimations and predictions using lognormal luminosity functions. For each cluster, we list the predicted number of potentially observable radio pulsars ($N_{\rm rad}$), the predicted total diffuse radio flux ($S_{\rm sim,tot}$) and the predicted gamma-ray luminosity ($L_{\gamma,\rm sim}$) for three different choices of efficiency (η_γ). See text for further details. To compute uncertainties in $N_{\rm rad}$, we assume that they are dominated by the statistical noise in the observed number of pulsars, $N_{\rm obs}$. The uncertainty in $N_{\rm rad}$ is then simply $N_{\rm rad}/\sqrt{N_{\rm obs}}$. For each model, we also list N_{10}, the total population estimate for these 10 GCs.

Cluster	$N_{\rm rad}$	$S_{\rm sim,tot}$ (mJy)	$L_{\gamma,\rm sim}$ (10^{34} erg s^{-1})		
			$\langle\eta_\gamma\rangle = 0.08$	$\langle\eta_\gamma\rangle = 0.06$	$\langle\eta_\gamma\rangle = 0.1$
Model 1 (FK06): $\mu = -1.1$ and $\sigma = 0.9$; $N_{10} = 688 \pm 82$					
47 Tuc	71 ± 19	3.1 ± 0.8	10 ± 5	7.7 ± 3.6	13 ± 6
M3	24 ± 12	0.16 ± 0.08	3.5 ± 2.2	2.6 ± 1.6	4.3 ± 2.7
M5	24 ± 11	0.31 ± 0.14	3.5 ± 2.1	2.6 ± 1.6	4.3 ± 2.6
M13	25 ± 11	0.38 ± 0.16	3.6 ± 2.1	2.7 ± 1.6	4.5 ± 2.6
Ter 5	167 ± 33	3.7 ± 0.7	24 ± 11	18 ± 8	30 ± 13
NGC 6440	88 ± 39	0.86 ± 0.4	13 ± 8	10 ± 6	16 ± 9
NGC 6517	46 ± 23	0.29 ± 0.15	6.6 ± 4.2	5.0 ± 3.1	8.3 ± 5.2
M28	120 ± 40	2.6 ± 0.9	17 ± 9	13 ± 7	22 ± 11
NGC 6752	44 ± 20	1.7 ± 0.8	6.3 ± 3.8	4.8 ± 2.8	7.9 ± 4.7
M15	79 ± 30	0.52 ± 0.20	11 ± 6	8.5 ± 4.6	14 ± 8
Model 2 (maximum $P_{\rm KS}$): $\mu = -0.61$ and $\sigma = 0.65$; $N_{10} = 453 \pm 56$					
47 Tuc	44 ± 12	2.2 ± 0.6	6.3 ± 3.0	4.8 ± 2.2	7.9 ± 3.8
M3	15 ± 8	0.11 ± 0.06	2.2 ± 1.4	1.6 ± 1.1	2.7 ± 1.8
M5	15 ± 7	0.20 ± 0.09	2.2 ± 1.3	1.6 ± 1.0	2.7 ± 1.6
M13	16 ± 7	0.24 ± 0.11	2.3 ± 1.3	1.7 ± 1.0	2.9 ± 1.7
Ter 5	100 ± 20	2.6 ± 0.5	14 ± 6	11 ± 5	18 ± 8
NGC 6440	68 ± 30	0.75 ± 0.33	9.8 ± 5.8	7.3 ± 4.3	12 ± 7
NGC 6517	30 ± 15	0.21 ± 0.10	4.3 ± 2.7	3.2 ± 2.1	5.4 ± 3.4
M28	85 ± 28	2.0 ± 0.7	12 ± 6	9.2 ± 4.7	15.3 ± 7.8
NGC 6752	27 ± 12	1.1 ± 0.5	3.9 ± 2.3	2.9 ± 1.7	4.9 ± 2.9
M15	53 ± 20	0.40 ± 0.15	7.6 ± 4.1	5.7 ± 3.1	9.5 ± 5.2
Model 3 (minimum χ^2): $\mu = -0.52$ and $\sigma = 0.68$; $N_{10} = 354 \pm 43$					
47 Tuc	37 ± 10	2.5 ± 0.7	5.3 ± 2.5	4.0 ± 1.9	6.6 ± 3.1
M3	12 ± 6	0.13 ± 0.06	1.7 ± 1.1	1.3 ± 0.8	2.2 ± 1.4
M5	13 ± 6	0.24 ± 0.11	1.9 ± 1.1	1.4 ± 0.8	2.3 ± 1.4
M13	14 ± 6	0.30 ± 0.13	2.0 ± 1.2	1.5 ± 0.9	2.5 ± 1.4
Ter 5	82 ± 16	2.9 ± 0.6	12 ± 5	8.9 ± 3.8	15 ± 6
NGC 6440	48 ± 21	0.74 ± 0.33	6.9 ± 4.0	5.2 ± 3.0	8.6 ± 5.1
NGC 6517	23 ± 12	0.21 ± 0.11	3.3 ± 2.1	2.5 ± 1.6	4.1 ± 2.7
M28	63 ± 21	1.5 ± 0.5	9.1 ± 4.6	6.8 ± 3.5	11 ± 6
NGC 6752	21 ± 10	1.2 ± 0.5	3.0 ± 1.8	2.3 ± 1.4	3.8 ± 2.3
M15	41 ± 15	0.43 ± 0.16	5.9 ± 3.2	4.4 ± 2.4	7.4 ± 3.9

$\sigma \sim 0.5$, however, lies well outside the χ^2 contours shown in Fig. 2. We therefore favour the region with $\mu \sim -1.1$ and $\sigma \sim 0.9$ (the nominal FK06 values), which is consistent with both constraints. In this case, the implied total number of pulsars $N_{\rm tot} \sim 150$ (see the lower panel of Fig. 6). Further constraints on these parameters, using a more detailed Bayesian analysis of these constraints for Terzan 5, will be the subject of a subsequent paper (Chennamangalam et al., in preparation).

Fig. 7 shows the analogous diagram to Fig. 6 for the power-law luminosity function for the choice $\beta = 1$. In this case, there is a wide range of $L_{\rm min}$ values that are consistent with the diffuse flux measurements (upper panel of Fig. 7), and no significant additional constraints on $L_{\rm min}$ can be made. The upper bound of $S_{\rm tot}$ gives an extremely high value of $N_{\rm tot} \sim 1000$, which seems unrealistic. However, the lower bound of $S_{\rm tot}$ gives $N_{\rm tot} = 340$ for $L_{\rm min} = 0.05$ mJy kpc^2 (lower panel of Fig. 7).

4.2 Predicted population sizes and diffuse fluxes for different GCs

The detection of diffuse gamma-ray emission from GCs has allowed some constraints to be placed on N_γ, the number of gamma-ray emitting pulsars in each cluster. Following Abdo et al (2010), we can write the total gamma-ray luminosity as follows:

$$L_\gamma = N_\gamma \langle \dot{E} \rangle \langle \eta_\gamma \rangle. \quad (8)$$

Here, $\langle \dot{E} \rangle$ is the average spin-down power of MSPs and $\langle \eta_\gamma \rangle$ is the average spin-down to gamma-ray luminosity conversion efficiency. As the values of $\langle \dot{E} \rangle$ and $\langle n_\gamma \rangle$ are not well known, Abdo et al (2010) assumed $\langle \dot{E} \rangle = (1.8 \pm 0.7) \times 10^{34}$ erg s^{-1} and $\langle \eta_\gamma \rangle = 0.08$. We use the values of N_γ estimated using the above relationship for the clusters with gamma-ray flux (and hence luminosity) measurements.

Table 3. Population estimations and predictions using power-law luminosity functions. See Table 2 for details about tabulated parameters.

Cluster	$N_{\rm rad}$	$S_{\rm sim,tot}$ (mJy)	$L_{\gamma,\rm sim}$ (10^{34} erg s^{-1}) $\langle\eta_\gamma\rangle = 0.08$	$\langle\eta_\gamma\rangle = 0.06$	$\langle\eta_\gamma\rangle = 0.1$
Model 4: $L_{\rm min} = 0.017$ and $\beta = 0.92$; $N_{10} = 3399 \pm 421$					
47 Tuc	313 ± 84	3.4 ± 0.89	45 ± 21	34 ± 16	56 ± 27
M3	114 ± 57	0.19 ± 0.09	16 ± 10	12 ± 8	21 ± 13
M5	112 ± 50	0.32 ± 0.14	16 ± 10	12 ± 7	21 ± 12
M13	118 ± 52	0.40 ± 0.18	17 ± 10	13 ± 8	21 ± 13
Ter 5	764 ± 153	4.4 ± 0.9	110 ± 48	83 ± 36	138 ± 60
NGC 6440	485 ± 217	1.2 ± 0.5	70 ± 41	53 ± 31	87 ± 52
NGC 6517	238 ± 119	0.35 ± 0.18	34 ± 22	26 ± 16	43 ± 27
M28	628 ± 209	2.5 ± 0.8	90 ± 46	68 ± 35	113 ± 58
NGC 6752	216 ± 97	1.9 ± 0.9	31 ± 19	23 ± 14	39 ± 23
M15	411 ± 155	0.68 ± 0.25	59 ± 32	449 ± 24	74 ± 40
Model 5: $L_{\rm min} = 0.022$ and $\beta = 1.01$; $N_{10} = 3767 \pm 478$					
47 Tuc	324 ± 87	3.3 ± 0.9	47 ± 22	35 ± 17	58 ± 28
M3	121 ± 61	0.19 ± 0.09	17 ± 11	13 ± 8	22 ± 14
M5	116 ± 52	0.31 ± 0.14	17 ± 10	13 ± 7	21 ± 12
M13	123 ± 55	0.39 ± 0.18	18 ± 11	13 ± 8	22 ± 13
Ter 5	815 ± 163	4.5 ± 0.9	117 ± 51	88 ± 39	147 ± 64
NGC 6440	580 ± 260	1.3 ± 0.6	84 ± 50	63 ± 37	104 ± 62
NGC 6517	271 ± 136	0.38 ± 0.20	39 ± 25	29 ± 19	49 ± 31
M28	714 ± 238	2.7 ± 0.9	103 ± 53	77 ± 30	129 ± 66
NGC 6752	237 ± 106	2.0 ± 0.9	34 ± 20	26 ± 15	43 ± 25
M15	466 ± 176	0.73 ± 0.27	67 ± 36	50 ± 27	84 ± 46
Model 6 (FG00): $L_{\rm min} = 0.03$ and $\beta = 0.85$; $N_{10} = 1590 \pm 194$					
47 Tuc	153 ± 41	3.2 ± 0.86	22 ± 10	17 ± 8	28 ± 13
M3	55 ± 28	0.18 ± 0.09	7.9 ± 5.1	5.9 ± 3.8	9.9 ± 6.3
M5	54 ± 24	0.31 ± 0.14	7.8 ± 4.6	5.8 ± 3.4	9.7 ± 5.7
M13	57 ± 26	0.38 ± 0.17	8.2 ± 4.9	6.2 ± 3.7	10 ± 6
Ter 5	363 ± 73	4.2 ± 0.8	52 ± 23	39 ± 17	65 ± 29
NGC 6440	216 ± 96	1.0 ± 0.5	31 ± 18	23 ± 14	39 ± 23
NGC 6517	112 ± 56	0.33 ± 0.16	16 ± 10	12 ± 8	21 ± 13
M28	287 ± 95	2.2 ± 0.7	41 ± 21	31 ± 16	52 ± 26
NGC 6752	101 ± 45	1.8 ± 0.8	15 ± 9	11 ± 6	18 ± 11
M15	192 ± 73	0.62 ± 0.23	28 ± 15	21 ± 11	35 ± 19

In Fig. 8, we compare the estimates of N_γ with our predicted numbers of radio pulsars ($N_{\rm rad}$) for one model of each luminosity function. A reasonable agreement can be noted for the lognormal function, but for the power-law function the values of $N_{\rm rad}$ are significantly larger than those of N_γ. This fact remains unchanged even if we choose other models from these luminosity functions (see Tables 2 and 3). Although this simple analysis does provide some support to the lognormal models, because of the assumptions made in equation (8) and implicitly assuming that $N_\gamma = N_{\rm rad}$, it does not help to constrain their values significantly.

By assuming $N_\gamma = N_{\rm rad}$, we obtain $L_{\gamma,\rm sim}$ from equation (8). We tabulate $L_{\gamma,\rm sim}$ for different choices of $\langle\eta_\gamma\rangle$ for different models in Tables 2 and 3. These values can be compared with observed values of L_γ and N_γ as shown in Table 4. It is apparent that the gamma-ray luminosities predicted by the power-law models are generally higher than observed. We note however that in addition to the explicit assumptions about beaming geometry mentioned above, it has recently been shown that the gamma-ray observations can be biased by one or more very bright pulsars in the cluster (Freire et al. 2011). They might not be representative of the diffuse flux of the whole population.

5 COMPARISON WITH EARLIER RESULTS

In Fig. 9, we compare our predicted number of pulsars, which have $L > 0.5$ mJy kpc^2 in different GCs using FK06 parameters, to those by HCT10. For Terzan 5, we do not use the distance they adopted for this cluster (10.3 kpc). Instead, here we recalculate the value of $N(L > 0.5)$ by adopting exactly the same method as HCT10 using the recent estimate 5.5 kpc (Ortolani et al 2007) to calculate the luminosities. The overall agreement is good, which again highlights the fact that, at least above 0.5 mJy kpc^2, the exact form of the luminosity function for GC pulsars is not uniquely specified by the current sample of luminosities.

HCT10 used their power-law luminosity functions to search for correlations between the number of inferred radio pulsars and fundamental cluster parameters. In their fig. 3, they present evidence for a correlation between $N_{\rm rad}$ and both cluster metallicity [Fe/H] and the two-body encounter rate $\Gamma_{\rm norm}$. An inspection of these diagrams suggests that the claimed correlations are strongly influenced by Terzan 5. For the purposes of this discussion, we adopt the parameters of model 1 (i.e. the lognormal luminosity parameters found by FK06), together with the revised distance to Terzan 5, and we

Table 4. Observed and inferred properties of GCs containing pulsars used in the present work. From left to right, we list the GC name, the distance from the Sun d and from the Galactic Centre $d_{\rm gcen}$ (both in kpc), the concentration parameter c (base-10 logarithm of the ratio of the tidal radius to core radius), the core radius $r_{\rm c}$ (pc), the base-10 logarithm of the central density ($\rho_{\rm c}$ in solar luminosities per cubic parsec), the velocity dispersion $v_{\rm c}$ (km s^{-1}), the base-10 logarithms of the cluster mass ($M_{\rm GC}$ in solar masses), the base-10 logarithms of the core relaxation time-scale [$t(r_{\rm c})$ in yr], the metallicity [Fe/H], the normalized two-body encounter rate $\Gamma_{\rm norm}$, the gamma-ray flux L_γ (10^{34} erg s^{-1}) and the inferred number of gamma-ray pulsars N_γ from Abdo et al (2010) and Tam et al. (2011). For $\Gamma_{\rm norm}$, we first calculate the two-body encounter rate for each GC as $\Gamma = \rho_{\rm c}^{1.5} {r_{\rm c}}^2$. The values of the core radius have been calculated as $r_{\rm c} = d\tan\theta_{\rm c}$, where $\theta_{\rm c}$ are the angular radii as quoted in the latest version of the Harris catalogue (Harris 1996, updated in 2010 December). The central cluster density $\rho_{\rm c}$ has been calculated as $\rho_{\rm c} = \Sigma_{\rm c}/(r_{\rm c}p)$ using the values of central surface brightness $\mu_{V{\rm c}}$ (in V magnitude per arcsec^2) and the extinction coefficient $A_V = 3.1\,E(B-V)$, where $E(B-V)$ is the colour excess. $\Sigma_{\rm c}$, the central surface brightness in $L_{V\odot}$ pc^2 can be calculated as $\log(\Sigma_{\rm c}) = 0.4[26.392 - (\mu_{V{\rm c}} - A_V)]$ and p is a parameter defined as $\log(p) = -0.603 \times 10^{-c} + 0.302$ (Djorgovski 1993). Finally, we normalized Γ to $\Gamma_{\rm norm}$ considering $\Gamma = 100$ for M62 (following Abdo et al 2010). The tabulated values for $v_{\rm c}$ and $\log(M_{\rm GC})$ can be found at http://www.astro.lsa.umich.edu/∼ognedin/gc/vesc.dat (Gnedin et al. 2002).

GC	d	$d_{\rm gcen}$	c	$r_{\rm c}$	$\log(\rho_{\rm c})$	$v_{\rm c}$	$\log(M_{\rm GC})$	$\log[t(r_{\rm c})]$	[Fe/H]	$\Gamma_{\rm norm}$	L_γ	N_γ
47 Tuc	4.03	7.4	2.07	0.42	4.93	16.4	6.17	7.84	−0.72	41.27	$4.8^{+1.1}_{-1.1}$	33^{+15}_{-15}
M3	10.23	12.0	1.89	1.10	3.58	9.2	5.98	8.31	−1.50	2.61	–	–
M5	7.76	6.2	1.73	0.99	3.87	11.8	5.93	8.28	−1.29	5.83	–	–
M13	7.13	8.4	1.53	1.28	3.55	10.3	5.89	8.51	−1.53	3.26	–	–
Ter 5	5.50	1.2	1.62	0.25	5.26	12.7	5.57	7.57	−0.23	46.50	$25.7^{+9.4}_{-8.8}$	180^{+100}_{-90}
NGC 6440	8.47	1.3	1.62	0.34	5.23	21.6	5.91	7.60	−0.36	78.27	$19.0^{+13.1}_{-5.0}$	130^{+100}_{-60}
NGC 6517	10.60	4.2	1.82	0.19	5.30	20.6	5.72	6.92	−1.23	29.71	–	–
M28	5.70	2.7	1.67	0.40	4.86	16.3	5.74	7.62	−1.32	28.19	$6.2^{+2.6}_{-1.8}$	43^{+24}_{-21}
NGC 6752	4.42	5.2	2.50	0.22	5.01	7.1	5.50	6.88	−1.54	14.72	$1.4^{+0.7}_{-0.7}$	10^{+15}_{-6}
M15	10.30	10.4	2.29	0.42	5.08	13.4	6.08	7.84	−2.37	66.81	<5.8	<56

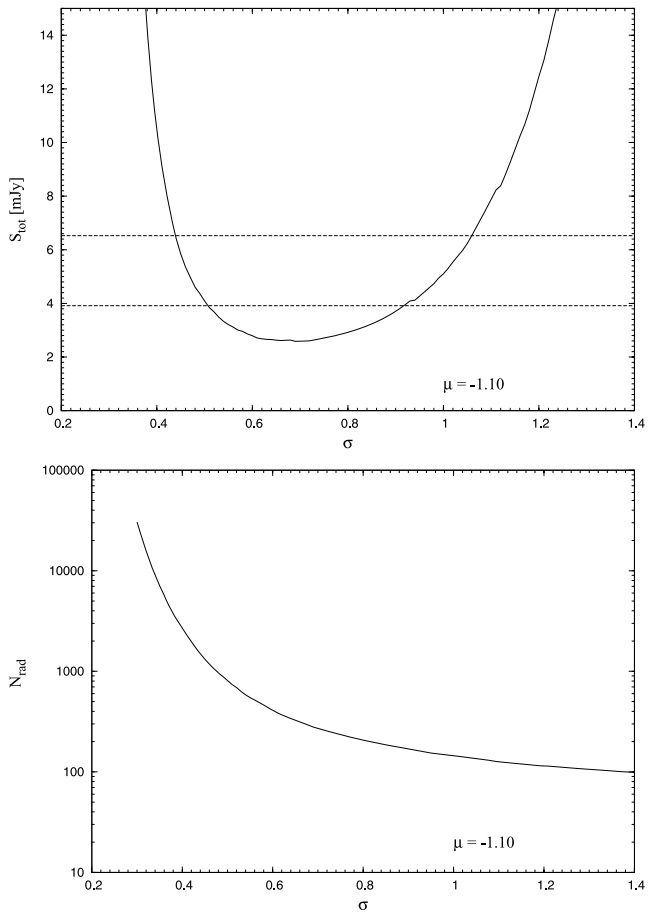

Figure 6. Variations of total radio flux (upper panel) and predicted number of pulsars (lower panel) in Terzan 5, as obtained from our simulations with a lognormal distribution, keeping μ fixed at -1.1 and varying σ. The dashed lines in the upper panel denote the ranges of $S_{\rm sim,tot} = S_{\rm obs,tot} \pm 25$ per cent.

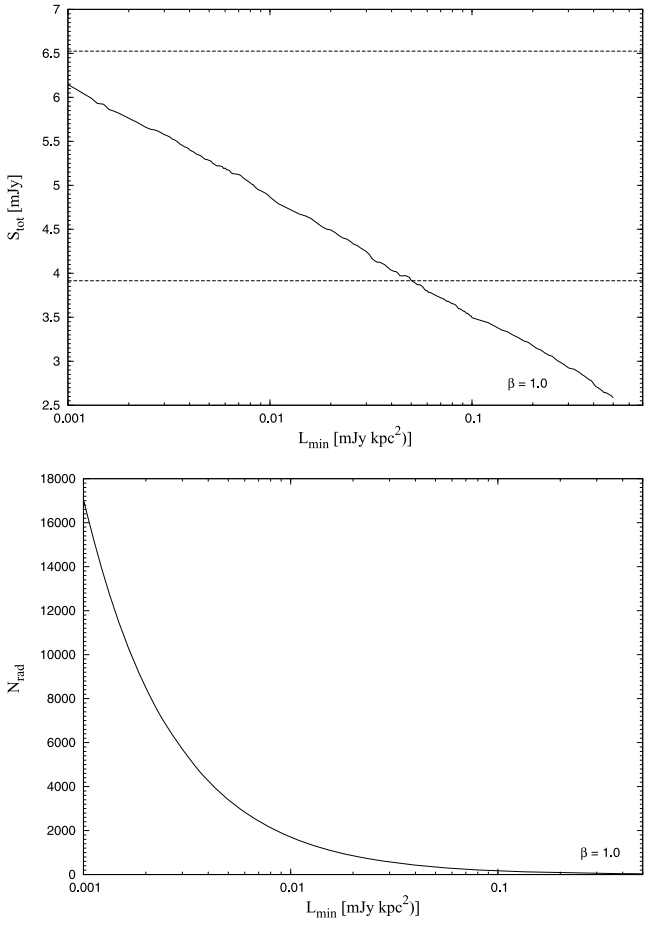

Figure 7. Variations of total radio flux (upper panel) and predicted number of pulsars (lower panel) in Terzan 5, as obtained from our simulations with a power-law distribution, keeping β fixed at 1.0 and varying $L_{\rm min}$. The dashed lines in the upper panel denote the ranges of $S_{\rm sim,tot} = S_{\rm obs,tot} \pm 25$ per cent.

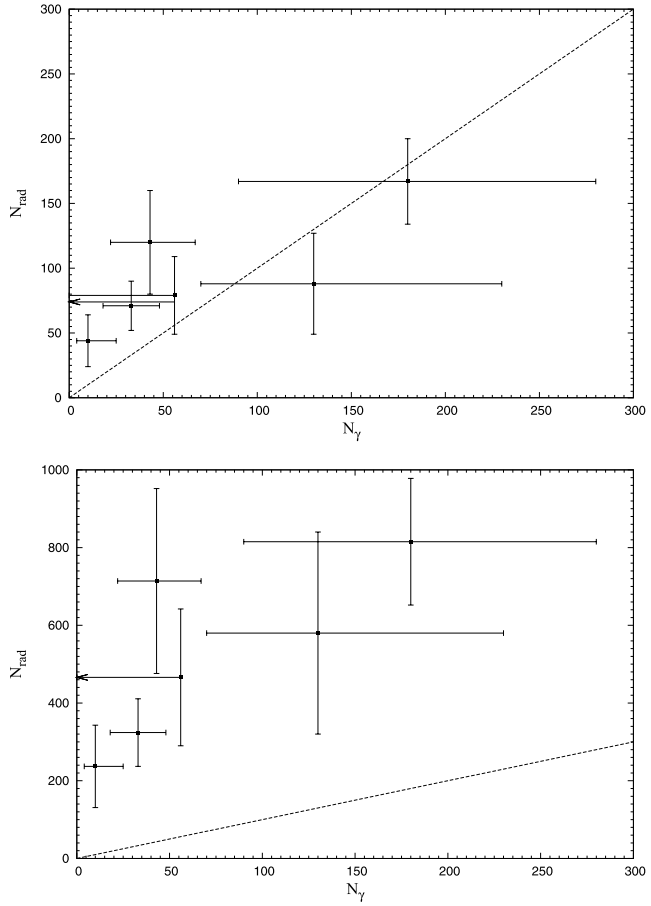

Figure 8. Comparison of the predicted number of pulsars from our simulations with those obtained from gamma-ray fluxes. Top: lognormal luminosity function (FK06 parameters). Bottom: power-law luminosity function (model 5).

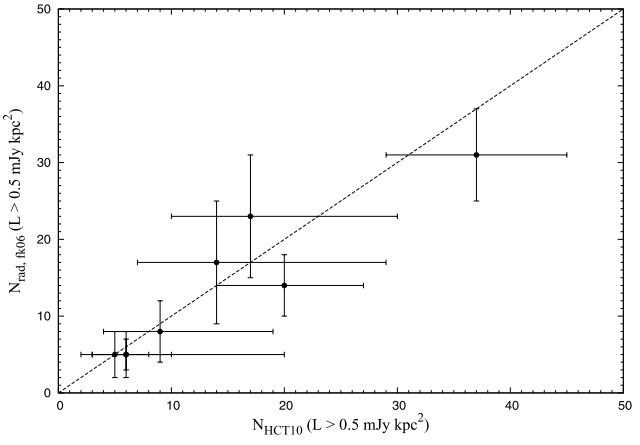

Figure 9. Comparison of our predicted number of pulsars in different GCs using FK06 parameters with those from HCT10.

revisit these proposed correlations in Fig. 10. Also shown here are the results of correlation tests between $N_{\rm rad}$ and other cluster parameters. We searched for relationships between the distance of each GC and the Galactic Centre $d_{\rm gcen}$, the logarithm of the central luminosity density $\rho_{\rm c}$, the concentration parameter[3] c, the logarithm of the core relaxation time $t(r_{\rm c})$, the cluster mass $M_{\rm GC}$, the central velocity dispersion $v_{\rm c}$ and the core radius $r_{\rm c}$. The parameter values used for this analysis are given in Table 4.

As can be seen in Fig. 10, none of the scatter diagrams provides compelling evidence for a direct relationship between $N_{\rm rad}$ and any cluster parameters. The lack of any statistically significant correlations can also be seen formally in Table 5, where we have calculated Pearson correlation coefficient (rp) and the probability at which the null hypothesis of zero correlation is disproved (P_{rp}), the Spearman correlation coefficient (rs) and the probability at which the null hypothesis of zero correlation is disproved (P_{rs}) and the Kendall τ and the probability at which the null hypothesis of zero correlation is disproved (P_τ).

We have shown the results of correlation analyses only for FK06 (our model 1), but for other models the results are almost the same. Because both the Spearman correlation and the Kendall τ test are based on ranks, in all the models the GCs with descending order of ranks (based on $N_{\rm rad}$) are Terzan 5, M28, NGC 6440, M15, 47 Tuc, NGC 6517, NGC 6752, M13, M3 and M5 (except for models 1 and 2, where there is a tie between M3 and M5, but the order of the other GCs is the same; see Tables 2 and 3). Even for the parametric test (Pearson correlation analysis), r_p always lies within 12 per cent of that of model 1 for Fe/H and within 14 per cent of that of model 1 for $\Gamma_{\rm norm}$. This also explains why our result contradicts that of HCT10 in spite of overall good agreement between the predicted numbers. According to HCT10, the GCs with descending order of ranks are Terzan 5, 47 Tuc, M28, NGC 6440, NGC 6441, NGC 6752, M13, M5 and M3, which is different from what we obtain.

6 CONCLUSIONS

We have modelled the observed luminosity distribution of millisecond pulsars in GCs as the brighter tail of a parent distribution. We have found that either a lognormal or a power-law distribution can be used as the parent distribution. We have demonstrated that a wide range of possible luminosity functions are compatible with the data, and that lognormal distribution functions provide a better match to the data than the traditionally favoured power-law distributions. In the light of these results, we conclude that there is currently no need to assume that the luminosity function for cluster pulsars is any different from that of pulsars in the Galactic disc found by FK06. Based on this result, it is quite possible that all pulsars follow a similar luminosity distribution, irrespective of their positions or recycling history.

Contrary to earlier claims by HCT10, we find no evidence for a significant correlation between the inferred numbers of radio pulsars in GCs and either metallicity or stellar encounter rate. No significant correlations were found with other cluster parameters either. Despite the lack of any obvious correlations found among this sample of 10 GCs, it is of great interest to perform an analysis using a much larger sample of clusters. Further constraints might be possible by incorporating observations of the diffuse gamma-ray flux, although this approach is complicated by model dependences in gamma-ray efficiency and the radio/gamma-ray beaming fraction.

One key difference between the two luminosity functions, which we have not yet commented on, is shown in Tables 2 and 3 by the tabulated parameter N_{10}, the sum of the population estimates

[3] This parameter is defined to be the logarithm of the ratio of the GC's tidal radius to its core radius.

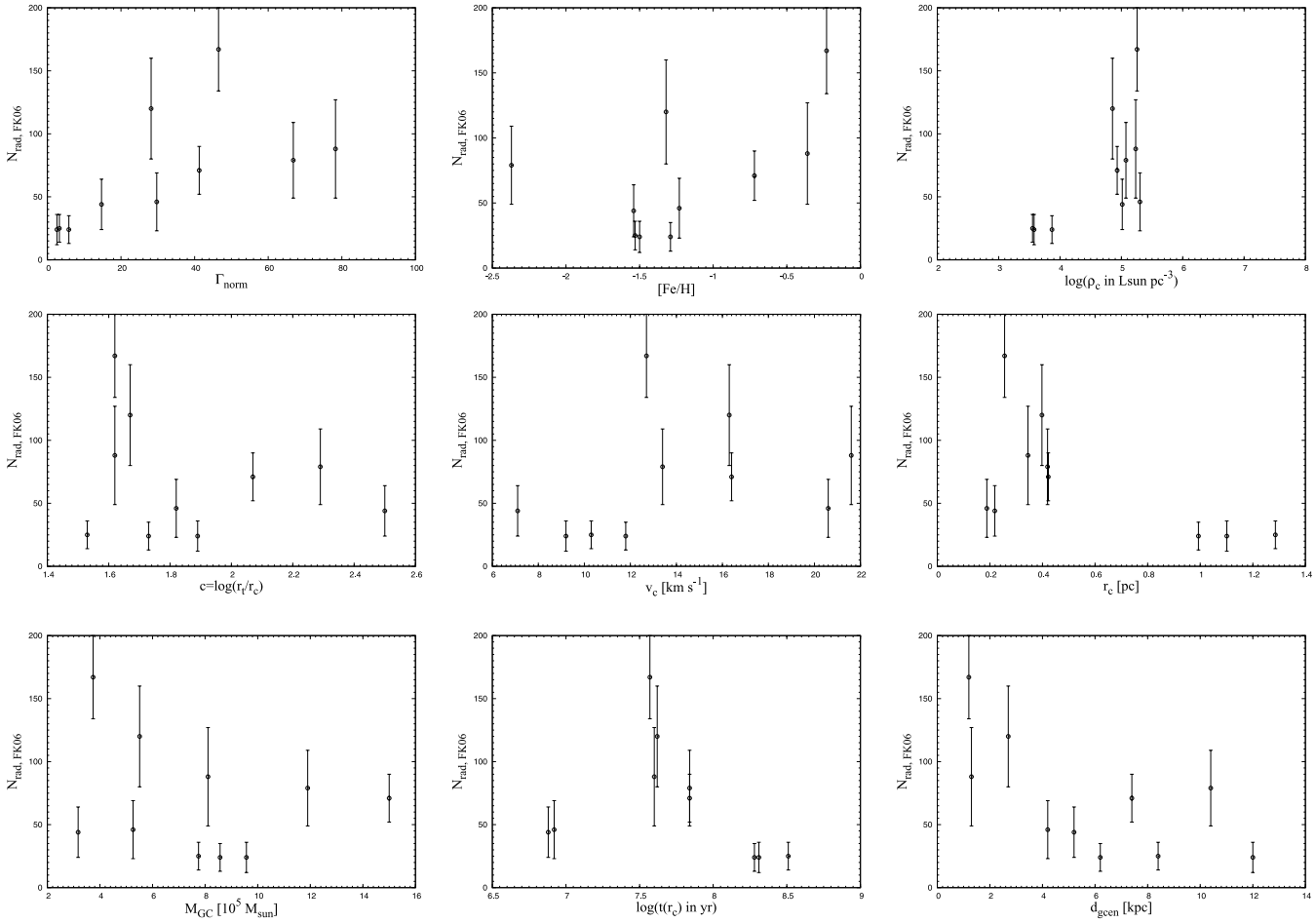

Figure 10. Plots of the predicted number of pulsars in different GCs using the FK06 parameters against various cluster parameters (see text).

Table 5. Results of different statistical correlation tests between the predicted number of pulsars with various GC parameters.

GC	Pearson		Spearman		Kendall	
property	rp	$P_{\rm rp}$	rs	$P_{\rm rs}$	τ	P_τ
$\Gamma_{\rm norm}$	0.60	0.07	0.80	0.02	0.67	0.01
Fe/H	0.51	0.13	0.44	0.18	0.31	0.21
$d_{\rm gcen}$	−0.64	0.04	−0.69	0.04	−0.54	0.03
$\log(\rho_{\rm c})$	0.64	0.04	0.62	0.06	0.45	0.07
c	−0.22	0.55	−0.24	0.48	−0.16	0.52
$\log[t(r_{\rm c})]$	−0.29	0.41	−0.51	0.13	−0.34	0.17
$M_{\rm GC}$	−0.25	0.48	−0.23	0.49	−0.22	0.37
$v_{\rm c}$	0.31	0.38	0.58	0.08	0.31	0.21
$r_{\rm c}$	−0.60	0.07	−0.52	0.12	−0.40	0.10

across all 10 GCs. As can be seen, the power-law models predict a systematically larger parent population than for the lognormal distribution (i.e. N_{10} in the range 1600–3800 compared to 350–700). This observation implies that the power-law distributions require larger birth rates over the lognormal models by a factor of 2–10. Although we defer a detailed population size analysis to a future paper, containing population estimates for more GCs, a simple scaling of these numbers to all 150 GCs that are currently known implies a population range for potentially observable recycled pulsars of 5000–11 000 pulsars in the lognormal models versus 24 000–57 000 for the power-law models. Assuming a recycled pulsar lifetime of $\sim 10^{10}$ yr, and a mean beaming fraction of 50 per cent, the implied birth rate of this population is at least 10^{-6} yr^{-1} over all Galactic GCs. Recent results concerning the low-mass X-ray binary (LMXB) population in GCs (see Pooley 2010; Heinke 2011, for reviews) suggest that there are of the order of 200 LMXBs in Galactic GCs. Assuming a typical LMXB lifetime of the order of 10^8 yr (Kulkarni & Narayan 1988), the implied birth rate is comparable to our rough estimates for the recycled pulsars, provided that the pulsar population estimates are closer to the ranges suggested by the lognormal models.

We consider this study to be the first step towards a more comprehensive analysis of the pulsar content of GCs. More detailed studies of the pulsar luminosity functions, which better account for the selection effects and detection issues in the various radio surveys, are still needed to further probe all these issues. In particular, in order to better understand this diverse population of neutron stars, we need to search for correlations between cluster parameters and the pulsar content beyond the small sample of 10 GCs considered here.

ACKNOWLEDGMENTS

We thank Craig Heinke and the anonymous referee for useful comments on an earlier version of the manuscript. This work was supported by a Research Challenge Grant to the WVU Center for Astrophysics by the West Virginia EPSCoR foundation, and also by

the Astronomy and Astrophysics Division of the National Science Foundation via a grant AST-0907967.

REFERENCES

Abdo A. A. et al., 2010, A&A, 524, 75
Alpar M. A., Cheng A. F., Ruderman M. A., Shaham J., 1982, Nat, 300, 728
Anderson S. B., 1993, PhD thesis, California Institute of Technology
Anderson S. B., Wolszczan A., Kulkarni S. R., Prince T. A., 1997, ApJ, 482, 870
Bagchi M., Lorimer D. R., 2010, in AIP Conf. Proc. 1357, Radio Pulsars: An Astronomical Key to Unlock the Secrets of the Universe. Am. Inst. Phys., New York, p. 173
Bagchi M., Ray A., 2009, ApJ, 693, L91
Bégin S., 2006, Masters Thesis, University of British Columbia
Bhattacharya D., Wijers R. A. M. J., Hartman J. W., Verbunt F., 1992, A&A, 254, 198
Biggs J. D., Bailes M., Lyne A. G., Goss W. M., Fruchter A. S., 1994, MNRAS, 267, 125
Boyles J., Lorimer D. R., Turk P. J., Mnatsakanov R., Lynch R. S., Ransom S. M., Freire P. C., Belczynski K., 2011, ApJ, in press (arXiv:1108.4402)
Camilo F., Lorimer D. R., Freire P., 2000, ApJ, 535, 975
Corongiu A., Possenti A., Lyne A. G., Manchester R. N., Camilo F., D'Amico N., Sarkissian J. M., 2006, ApJ, 653, 1417
D'Amico N., Lyne A. G., Manchester R. N., Possenti A., Camilo F., 2001, ApJ, 548, L171
Djorgovski S., 1993, in Djorgovski S. G., Meylan G., eds, ASP Conf. Ser. Vol. 50, Structure and Dynamics of Globular Clusters. Astron. Soc. Pac., San Francisco, p. 373
Faucher-Giguère C. A., Kaspi V. M., 2006, ApJ, 643, 332 (FK06)
Foster R. S., Fairhead L., Backer D. C., 1991, ApJ, 378, 687
Freire P. C. C., Ransom S. M., Gupta Y., 2007, ApJ, 662, 1177
Freire P. C. C., Wolszczan A., van den Berg M., Hessels J. W. T., 2008a, ApJ, 679, 1433
Freire P. C. C., Ransom S. M., Bégin S., Stairs I. H., Hessels J. W. T., Frey L. H., Camilo F., 2008b, ApJ, 675, 670
Freire P. C. C., Parent D., 2011, The Fermi Timing Consortium. Sci, submitted
Fruchter A. S., Goss W. M., 2000, ApJ, 536, 865
Gnedin O. Y., Zhao H., Pringle J. E., Fall S. M., Livio M., Meylan G., 2002, ApJ, 568, L23
Gonthier P. L., Ouellette M. S., Berrier J., O'Brien S., Harding A. K., 2002, ApJ, 565, 482
Harris W. E., 1996, AJ, 112, 1487
Heinke C., 2011, in Kalogera V., van der Sluys M., eds, AIP Conf. Proc. 1314, International Conference on Binaries: In celebration of Ron Webbink's 65th birthday. Am. Inst. Phys., New York, p. 135
Hessels J. W. T., Ransom S. M., Stairs I. H., Freire P. C. C., Kaspi V. M., Camilo F., 2006, Sci, 311, 1901
Hessels J. W. T., Ransom S. M., Stairs I. H., Kaspi V. M., Freire P. C. C., 2007, ApJ, 670, 363
Hobbs G., Faulkner A., Stairs I. H., 2004, MNRAS, 352, 1439
Hui C. Y., Cheng K. S., Taam R. E., 2010, ApJ, 714, 1149 (HCT10)
Ivanova N., Heinke C. O., Rasio F. A., Belczynski K., Fregeau J. M., 2008, MNRAS, 386, 553
Katz J. I., 1975, Nat, 253, 698
Kramer M., Xilouris K. M., Lorimer D. R., Doroshenko O., Jessner A., Wielebinski R., Wolszczan A., Camilo F., 1998, ApJ, 501, 270
Kulkarni S. R., Narayan R., 1988, ApJ, 335, 755
Kulkarni S. R., Anderson S. B., Prince T. A., Wolszczan A., 1991, Nat, 349, 47
Lorimer D. R., Kramer M., 2005, Handbook of Pulsar Astronomy. Cambridge Univ. Press, Cambridge
Lorimer D. R., Bailes M., Dewey R. J., Harrison P. A., 1993, MNRAS, 263, 403
Lorimer D. R., Yates J. A., Lyne A. G., Gould D. M., 1995, MNRAS, 273, 411
Lynch R. S., Ransom S. M., Freire P. C. C., Stairs I. H., 2011, ApJ, 734, 89
Lyne A. G., Brinklow A., Middleditch J., Kulkarni S. R., Backer D. C., 1987, Nat, 328, 399
Lyne A. G., Johnston S., Manchester R. N., Staveley-Smith L., D'Amico N., 1990, Nat, 347, 650
Lyne A. G., Biggs J. D., Harrison P. A., Bailes M., 1993, Nat, 361, 47
Lyne A. G., Manchester R. N., D'Amico N., 1996, ApJ, 460, L41
McConnell D., Deshpande A. A., Connors T., Ables J. G., 2004, MNRAS, 348, 1409
Maron O., Kijak J., Kramer M., Wielebinski R., 2000, A&AS, 147, 195
Ortolani S., Barbuy B., Bica E., Zoccali M., Renzini A., 2007, A&A, 470, 1043
Pooley D., 2010, in Comastri A., Angelini L., Cappi M., eds, AIP Conf. Ser. Vol. 1248, X-ray Astronomy 2009: Present Status, Multiwavelength Approach and Future Perspectives. Am. Inst. Phys., New York, p. 187
Possenti A., D'Amico N., Manchester R. N., Camilo F., Lyne A. G., Sarkissian J., Corongiu A., 2003, ApJ, 599, 475
Press W. H., Teukolsky S. A., Vetterling W. T., Flannery B. P., 2007, Numerical Recipes: The Art of Scientific Computing. Cambridge Univ. Press, Cambridge
Ransom S. M., Greenhill L. J., Herrnstein J. R., Manchester R. N., Camilo F., Eikenberry S. S., Lyne A. G., 2001, ApJ, 546, L25
Ransom S. M., Stairs I. H., Backer D. C., Greenhill L. J., Bassa C. G., Hessels J. W. T., Kaspi V. M., 2004, ApJ, 604, 328
Ransom S. M., Hessels J. W. T., Stairs I. H., Freire P. C. C., Camilo F., Kaspi V. M., Kaplan D. L., 2005, Sci, 307, 892
Ridley J. P., Lorimer D. R., 2010, MNRAS, 404, 1081
Robinson C., Lyne A. G., Manchester R. N., Bailes M., D'Amico N., Johnston S., 1995, MNRAS, 274, 547
Romani R. W., Kulkarni S. R., Blandford R. D., 1987, Nat, 329, 309
Tam P. H. T., Kong A. K. H., Hui C. Y., Cheng K. S., Li C., Lu T. N., 2011, ApJ, 729, 90
Toscano M., Bailes M., Manchester R. N., Sandhu J. S., 1998, ApJ, 506, 863
Verbunt F., van den Heuvel E. P. J., van Paradijs J., Rappaport S. A., 1987, Nat, 329, 312
Wolszczan A., Kulkarni S. R., Middleditch J., Backer D. C., Fruchter A. S., Dewey R. J., 1989, Nat, 337, 531

This paper has been typeset from a TEX/LATEX file prepared by the author.